[10]. However, there are two phases in this case (Table 1). This suggests that the mechanism of columnar structure is not described by the model of Thornton. Further, we shall consider different generating mechanisms of these structures. Not without interest is the comparison of the results obtained with the specific data on the nanoindentation of other materials. These data are presented in Table 2.

Table 2. Properties of the materials according to the calculated nanoindentation [11].

Material	H, GPa	E, GPa	R, %
Copper	2.1	121	14
Titanium	4.1	130	19
The multilayer film Ti/α-C:H	8.0	128	34
The amorphous ribbon Zr-Cu-Ti-Ni	11.5	117	42
Silicon (100)	11.8	174	62
Thin film Ti-Si-N	28.4	295	62

The following notations are used in Table 2: *H* is hardness, *E* is Young's modulus and *R* is elastic recovery.

We obtained the result of 7.413 GPa. Table 2 shows that the nanohardness of coating Cr-Mn-Si-Cu-Fe-Al is almost 2 times higher than that of titanium and is almost the same as for multilayer film Ti/α-C:H. However, preparation of such film is more difficult than that of coating Cr-Mn-Si-Cu-Fe-Al with a composite cathode. The nanohardness of coating Cr-Mn-Si-Cu-Fe-Al+Ti (14.2 GPa) is nearly equal to the nanohardness of amorphous ribbon Zr-Cu-Ti-Ni (14.5 GPa) or silicon (100) (14.8 GPa).

Thus, the relationship between the coating structure and its hardness is revealed. A coating hardness increases for ordered structures. The relationship between the coating hardness and its structure was discussed in [12].

The cellular substructure is often formed in solidifying due to concentration supercooling (Fig. 3).

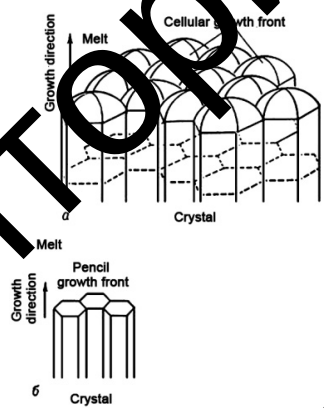

Fig. 3. (a) The cellular structure and (b) pencil (columnar) structure [13].

If a supramatal liquid zone having impurity elements is formed with a cellular structure formation at the solidification front, then the impurity segregation occurrence at the cell boundary arises due to the lateral diffusion impurities flux from the top of the growing projection. The amount of impurity reaching the border of the cell is difficult to measure, this amount depending on the depth of the recess between the cells. The recesses between the cells become deeper as supercooling rises, this being led to the enrichment of cell boundaries with impurity because of impurity diffusion from the top of the cell. The concentration of impurities on the boundary can be several times higher than the concentration in the center of the cell.

The cellular structure consists of a series of parallel elements having the shape of rods and being spaced in the direction of crystallization (Fig. 3). The rods are of a cross sectional shape of regular hexagons and the structure at the solidification front is an aggregate of hexagonal cells. The upper free surface of crystals having such a structure is wavy.

In this case (Fig. 1 and 2) concave cells are observed. A negative gradient of impurity concentration makes it possible.

To address the issue of self-organization of the coating structural units let us consider Bénard cell model. Bénard cells are ordered hexagonally or having a form of cylindrical shafts convection cells in viscous medium with a vertical temperature gradient (Fig. 4).

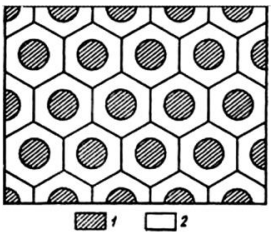

Fig. 4. Scheme of Bénard cells:1 – upward movement, 2 – downward movement.

Bénard cells are one of the three standard examples of self-organization along with the laser and the Belousov-Zhabotinsky reaction. The temperature gradient is the control parameter of self-organization. Heating of an initially homogeneous liquid layer results in diffusion due to density variation.

In overcoming some critical value of the gradient, diffusion does not cause thermal uniformity by volume. Cylindrical shafts rotating in opposite directions (as a clutch gear) originate. The second critical transition originates under gradient temperature increase. In order to accelerate the diffusion, each shaft falls into two smaller shafts. As the control parameter increases the shafts are broken down, the turbulent chaos arises in the region. Analyzing processes in Bénard system the Rayleigh number is selected as a control parameter: $\mathrm{Re} = gL^3bdT/va$, where g is a gravity factor, L is a specific size, b is a coefficient of volume expansion, dT is a temperature gradient, v is a kinematic viscosity, and a is a coefficient of thermal environment.

For the formation of Benard cells it is necessary that the number of Re = 10 ... 20. Let us estimate the Rayleigh number in this case: $L \approx 10^{-3}$ m, $b \approx 11\ 10^{-6}$ K^{-1}, $dT \approx 103$ K, $\nu \approx 10^{-6}$ Pa m^3 s/kg and $\approx 8\ 10^{-6}$ m^2/s, we obtain Re ≈ 14. Thus, the formation of Benard cells in the formation of coatings Cr-Mn-Si-Cu-Fe-Al+Ti is possible.

Let us consider the formation of a cellular structure using the model of YADS-cellular dislocation structure [14]. Plastic deformation of crystals (and coatings) is accompanied by the formation of strain relief on the surface, reflecting the strain localization process in the crystal on the meso, micro and nanoscale level. YADS begins to take shape in a deformed crystal at the end of the second and beginning of the third stage of metals strain hardening curve and finishes at the end of the third stage (see [14] and the references therein). With further deformation of the material a fragmented dislocation structure - FDR is formed (at the fourth and fifth stages of strain hardening curve). YADS is believed to be a process of self-organization of dislocations in a multiple slip. A certain criteria should be satisfied for its occurrence (as is in case of Bénard cells), this criteria linking reproductive factors, immobilization and annihilation of dislocations.

In the process of ion-plasma coating and cooling, strained states are formed in the coating, these states possibly being the sources of dislocations throughout the volume of the deposited coating [15]. A sharp increase in the microhardness of the formed film is the result of dislocation hardening of the coating material.

5. Practical applications

The technique of applying ion-plasma corrosion resistant coatings can be divided into several stages, namely, control, preparation, parts cleaning, corrosion-resistant layer spraying and control stages.

The control step involves checking accompanying papers to verify the material grade and the parts in a lot subjected to anti-corrosion treatment. In addition the absence of mechanical damage to the parts is checked. The hardness of a test specimen is measured. The second step includes preparing the in-process parts and the coating unit chamber. The parts are washed with gasoline, wiped dry, then washed with alcohol and wiped dry again. The chamber from the inside is treated with gasoline and alcohol, and the chamber is pumped to the pressure of (2-5) × 10^{-2} Pa. The parts cleaning is carried out in the chamber by glow discharge first, the voltage of (3-6) kV is applied over a period of 5 or 10 minutes followed by ionic cleaning of the parts. The chamber is evacuated to the pressure of 6×10^{-3} Pa, argon gas is fed to the pressure of $(4\text{-}6)\times10^{-2}$ Pa, and the discharge voltage of (700-800) V is set. The ionic cleaning is carried out over a period of 15-20 min. When the pressure of 6×10^{-3} Pa in the chamber is reached, nitrogen to the pressure of $(6\text{-}9)\times10^{-2}$ Pa is fed into the chamber, the voltage of (900-1000) kV is set and the coating is sputtered. It takes 2 hours to complete the process.

In the procedure described the parts subjected to coating were those of mining equipment. Parts testing had been carried out at the enterprises of JSC "Mittal Steel Temirtau" for 8 months, as well as in the laboratory in excited environment by the method described in GOST 9.008-82 ESZKS (Table. 3).

Table 3 shows that the developed technology of anti-corrosion coatings gives good results of corrosion resistance.

Table 3. Parts characteristics of JSC "Mittal Steel Temirtau" with anticorrosive coatings.

Name of part	Anti-corrosion coating	Service life increase
Stem, Steel 40X	Cr-Mn-Si-Cu-Fe-Al+Ti	5 times
Nipple 12, Steel 35	Cr-Mn-Si-Cu-Fe-Al+Ti	15 times
Clutch 12, Steel 35	Cr-Mn-Si-Cu-Fe-Al+Ti	15 times
RU11.008-01 Coupling, Steel 35	Cr-Mn-Si-Cu-Fe-Al+Ti	15 times
HLG Cork 30, Steel 35	Cr-Mn-Si-Cu-Fe-Al+Ti	15 times
Elbow 10NG12, Steel 35	Cr-Mn-Si-Cu-Fe-Al+Ti	15 times
Cheek right 9.00.00.018 Steel 3	Cr-Mn-Si-Cu-Fe-Al+Ti	15 times

6. Conclusion

Comparing the obtained nanohardness of (7.413 GPa) with the familiar solid materials shows that the nanohardness of coating Cr-Mn-Si-Cu-Fe-Al is almost 2 times higher than the titanium nanohardness and almost the same as for multilayer film Ti/α-C:H. However, preparation of such film is more difficult than that of coating Cr-Mn-Si-Cu-Fe-Al with a composite cathode, which can be easily obtained by induction melting.

The formation of a cellular structure of coating Cr-Mn-Si-Cu-Fe-Al-Ti deposited in the nitrogen environment is not a trivial issue. The formation of the structure fits into these models: concentration supercooling in the presence of the radial gradient of titanium nitride and chromium impurity concentration; Bénard cells, being caused by the presence of the vertical temperature gradient; cellular dislocation structure associated with the presence of plastic strain in the coating.

The results of this work were used in the development of technology and the application of anti-corrosion wear-resistant coatings on parts of mining and oilfield equipment. It is possible to increase the service life of the equipment and give a significant economic effect.

In the long run, it is possible to replace scarce and expensive grades of steel used for manufacturing various parts of mining and oilfield equipment with cheaper steel coatings being proposed.

References

[1] D. Lorpez, N. Alonso Falleiros, A.P. Tschiptschin, Effect of nitrogen on the corrosion–erosion synergism in an austenitic stainless steel, Tribology International, 2011, Vol. 44, pp. 610–616.

[2] R. Liu, X. Li, X.Hu, H. Dong, Surface modification of a medical grade Co-Cr-Mo alloy by low-temperature plasma surface alloying with nitrogen and carbon, Surface and Coatings Technology, 2013, Vol. 232, pp. 906-911.
[3] J. Klemm, S.O. Klemm, M.J. Duarte et. al., Multi-element-resolved electrochemical corrosion analysis. Part I. Dissolution behavior and passivity of amorphous Fe50Cr15Mo14C15B6 , Corrosion Science, 2014, Vol. 89, pp. 59-68.
[4] R. Alvarez-Asencio, M. Sababi, J. Pan, et. al., Role of microstructure on corrosion initiation of an experimental tool alloy: A Quantitative Nanomechanical Property Mapping study, Corrosion Science, 2014, Vol. 89, pp. 236-241.
[5] F. Otto, Y. Yang , H. Bei, E. P. George, Relative effects of enthalpy and entropy on the phase stability of equiatomic high-entropy alloys, Acta Materialia, 2013, Vol. 61, pp. 2628-2638.
[6] M.H. Tsai, J.W. Yeh, High-entropy alloys: a critical review, Mater. Res. Lett., 2014, Vol. 2, pp. 107-123.
[7] A.D. Pogrebnyak, A.A. Baghdasaryan, I.V. Yakovenko, V.M. Beresnev, Structure and properties of high entropy alloys and nitride coatings on their basis, Russian Chemical Reviews, 2014, Vol. 83, №11, 1027-1061.
[8] B.Schuh, F. Mendez-Martin, B. Vulker, et. al., Mechanical properties, microstructure and thermal stability of a nanocrystalline CoCrFeMnNi high-entropy alloy after severe plastic deformation, Acta Materialia, 2015, Vol. 96, pp. 258-268.
[9] J.A. Thornton, Structure and topography of sputtering coatings, Ann. Rev. Material Sci.,1977,Vol. 7, pp. 239-260.
[10] O.V. Sobol, A.A. Andreev, V.F. Gorban and others, On the reproducibility of single-phase structural state multielement highentropy system Ti-V-Zr-Nb-Hf and high hard nitrides based on it as they are formed by vacuum arc method, Technical Physics Letters, 2012, vol. 38, no. 13, pp. 40-47 (In Russian).
[11] Y.I. Golovin, Nanoindentation and mechanical properties of solids in submikroobëmah, thin surface layers and films, Solid State Physics, 2008, V. 50, Vol. 12, pp. 2113 – 2142 (In Russian).
[12] J. Musil, H. Polakova, Hard nanocomposite Zr-Y-N coatings, correlation between hardness and structure, Surface and Coatings Technology, 2000, V. 127, pp. 99-106.
[13] W. Vayngard, Introduction to the physics of crystallization of metals, M, Mir, 1967, 170 p.
[14] G.A. Maligin, Modelling of deformation of the surface relief plastically deformable crystal, Solid State Physics (Russia), 2007, V. 49, №. 8, pp. 1392-1397 (In Russian).
[15] V.A. Barvinok, Managing stress state and properties of plasma coatings, M., Engineering, 1990, 384 p.